Magn. Reson., 3, 161–168, 2022
https://doi.org/10.5194/mr-3-161-2022

Open Access
MAGNETIC RESONANCE

Reverse dynamic nuclear polarisation for indirect detection of nuclear spins close to unpaired electrons

Nino Wili[1], **Jan Henrik Ardenkjær-Larsen**[2], **and Gunnar Jeschke**[1]

[1]Department of Chemistry and Applied Biosciences, Laboratory of Physical Chemistry, ETH Zurich, Vladimir-Prelog-Weg 2, 8093 Zurich, Switzerland
[2]Department of Health Technology, Center for Hyperpolarization in Magnetic Resonance, Technical University of Denmark, Building 349, 2800 Kgs Lyngby, Denmark

Correspondence: Nino Wili (nino.wili@alumni.ethz.ch)

Received: 22 June 2022 – Discussion started: 27 June 2022
Revised: 1 August 2022 – Accepted: 1 August 2022 – Published: 10 August 2022

Abstract. Polarisation transfer schemes and indirect detection are central to magnetic resonance. Using the trityl radical OX063 and a pulse electron paramagnetic resonance spectrometer operating in the Q-band (35 GHz, 1.2 T), we show here that it is possible to use pulsed dynamic nuclear polarisation (DNP) to transfer polarisation from electrons to protons *and back*. The latter is achieved by first saturating the electrons and then simply using a reverse DNP step. A variable mixing time between DNP and reverse DNP allows us to investigate the decay of polarisation on protons in the vicinity of the electrons. We qualitatively investigate the influence of solvent deuteration, temperature, and electron concentration. We expect reverse DNP to be useful in the investigation of nuclear spin diffusion and envisage its use in electron–nuclear double-resonance (ENDOR) experiments.

1 Introduction

Polarisation or coherence transfer schemes are fundamental to modern magnetic resonance (Ernst et al., 1987). Most commonly, these are insensitive nuclei enhanced by polarisation transfer (INEPT) in liquid-state nuclear magnetic resonance (NMR), cross polarisation (CP) in solid-state NMR, and dynamic nuclear polarisation (DNP) to transfer electron spin polarisation to nuclear spins. The enhanced polarisation leads to an improved signal-to-noise ratio. Additionally, spins with a higher gyromagnetic ratio often show faster longitudinal relaxation; thus, the necessary relaxation delay between repetitions of the same experiment can be reduced. This further leads to a higher sensitivity per unit time.

However, this is only half the story. Rather often in NMR, after an initial transfer from high-γ nuclei (usually protons) to heteronuclei as well as an evolution period on the latter, the magnetisation is transferred back to the initial spin and then detected. This is referred to as indirect detection. Again, this leads to increased sensitivity, but it also allows one to establish correlations if the spectrum of the initial spins is resolved.

DNP is now an established technique for polarisation enhancement of nuclear spins (Ni et al., 2013; Lilly Thankamony et al., 2017). The polarisation of electrons, which are either naturally present in the sample under investigation or are added to it, is transferred to nuclei by appropriate microwave irradiation schemes. At high fields ($\gtrapprox 3.5$ T), continuous-wave (CW) irradiation provided by gyrotrons is usually used, and the transfer is quite slow due to the low microwave power available at high frequencies. Recently, several groups have introduced schemes using broadband frequency-swept excitation (Hovav et al., 2014; Bornet et al., 2014; Kaminker and Han, 2018; Gao et al., 2019; Shimon and Kaminker, 2020). At lower fields and frequencies, quite an appreciable number of pulsed DNP variants are already available (Henstra et al., 1988; Tan et al., 2019a, c; Redrouthu and Mathies, 2022). A very simple and efficient one is nuclear orientation via electron spin locking (NOVEL), in which the electron is spin locked with a nutation frequency corresponding to the nuclear Zeeman frequency (Henstra et al., 1988). It is worth noting that the electron–nuclear polarisation transfer is achieved without any radio frequency

(rf) irradiation of the nuclei. This is in contrast to CP, in which both spins are irradiated with the same nutation frequency. The NOVEL condition is sometimes also referred to as a rotating frame–laboratory frame Hartmann–Hahn matching (Can et al., 2015).

In principle, electron–nuclear polarisation transfer should be possible in both directions. In this work, using trityl OX063 in protonated and deuterated solvents as an example (a sample well suited for pulsed DNP; Mathies et al., 2016), we show that this is indeed the case. After an initial DNP step, the electron spins are saturated. This leads to a situation where the nuclear polarisation is larger than the electron spin polarisation. A second DNP step then causes nuclear–electron polarisation transfer. We refer to this as "reverse DNP". The experiments are performed at 80 K on a home-built electron paramagnetic resonance (EPR) spectrometer based on a fast arbitrary waveform generator (AWG) (Doll and Jeschke, 2017) working in the Q-band ($\approx$ 35 GHz, 1.2 T), corresponding to a proton resonance frequency of about 50 MHz.

A variable waiting time between DNP and reverse DNP allows us to study the decay of nuclear polarisation close to the unpaired electron. As expected, the nuclear polarisation decays much slower than the longitudinal relaxation of the electron spin $T_{1,e}$. Preliminary results show a profound influence of protonation of the solvent, indicating that spin diffusion away from the paramagnetic centre plays an important role. The proton polarisation decay is enhanced when increasing the trityl concentration from 100 µM to 5 mM. Finally, periodic inversion of the electron spin also accelerates the decay. We interpret this as an increase in spin diffusion away from the paramagnetic centre due to hyperfine decoupling.

The method has potential with respect to investigating the influence of spin diffusion away from a paramagnetic centre (Wolfe, 1973; Stern et al., 2021; Tan et al., 2019b; Jain et al., 2021). On the other hand, we envisage the use of reverse DNP in electron–nuclear double-resonance (ENDOR) experiments of nuclei with substantial hyperfine couplings (Harmer, 2016; Rizzato et al., 2013).

2 NOVEL matching and electron depolarisation

In a first step, we investigate the electron spin depolarisation during DNP using the NOVEL sequence.

There are several ways one can determine the NOVEL condition experimentally; for example, one could perform nutation experiments and then set the microwave amplitude to the desired nutation frequency. In this work, we used a simple spin-lock sequence followed by a spin echo, as in van den Heuvel et al. (1992) (see Fig. 1a).

The echo intensity as a function of the spin-lock strength (with a constant pulse length of 2 µs) is shown in Fig. 1b. For a vanishing nutation frequency, there is no effective spin lock and, accordingly, no echo intensity. The intensity is then

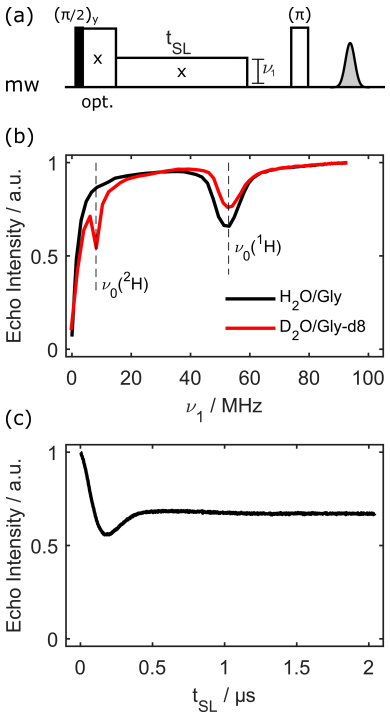

Figure 1. Electron spin depolarisation during electron spin locking. Panel **(a)** displays the pulse sequence. The spin lock can optionally start at full power to purge off-resonance effects. Panel **(b)** shows the depolarisation power (or nutation frequency) matching with a fixed spin-lock length of $t_{SL} = 2\,\mu s$ for 100 µM OX063 at 80 K. Panel **(c)** presents the electron depolarisation curve for the sample in protonated solvent, with the microwave power adjusted to the proton Larmor frequency, $\nu_1 = \nu_0(^1H)$, as determined in panel **(b)**.

more or less constant if the nutation frequency is larger than the trityl electron spin resonance (ESR) linewidth ($\approx$ 12 MHz full width at half maximum, FWHM, at 1.2 T). However, if the NOVEL condition is fulfilled, there is a drop in electron spin echo intensity, as polarisation is transferred to nearby nuclei. In fully protonated solvent, there is only a dip at $\nu_1 = \nu_0(^1H)$. In deuterated solvent, there is an additional dip at $\nu_1 = \nu_0(^2H)$.

The transfer can further be investigated by keeping the spin-lock power fixed on the NOVEL condition and increasing the spin-lock pulse length t_{SL}. This is shown for the protonated solvent in Fig. 1c. Note that the sequence was slightly adjusted in this case. At the NOVEL condition, the spin-lock power is of the same order as the EPR linewidth; thus, transient nutations due to off-resonance effects obscure the electron–nuclear transfer dynamics (see the Supplement). This can be alleviated by starting the spin lock at full power for about 500 ns, at which point the transient nutations have decayed. The spin-lock amplitude is then suddenly dropped from maximum power to the NOVEL condition. This corresponds to $t = 0$ in Fig. 1c. The transfer curve shows clear transient behaviour, with a minimum of the electron spin

echo intensity at 184 ns. This is consistent with earlier investigations of DNP with trityl radicals (Mathies et al., 2016).

In principle, this transfer could be repeated several times in order to accumulate nuclear polarisation. This is usually done for pulse DNP experiments with direct NMR detection. The effect of multiple NOVEL contacts on the depolarisation is further investigated in the Supplement (Sect. S9), but all further experiments were conducted with single DNP contacts, as the aim was not a simple NMR signal enhancement but rather to investigate the spin dynamics.

3 Electron saturation and repolarisation by reverse DNP

The flip-flop terms in the effective Hamiltonian during NOVEL matching lead to an oscillation of the *difference* in electron and nuclear polarisation (P_E and P_N respectively). Usually, the electron polarisation is much larger ($|P_E| \gg |P_N|$) such that polarisation is transferred from electrons to nuclei. However, if we saturate the electron spins after a DNP transfer, the nuclear polarisation is larger than the electron spin polarisation ($|P_E| < |P_N|$). In this situation, DNP leads to a nuclear–electron polarisation transfer. The pulse sequence for this is shown in Fig. 2a. It starts as before with a NOVEL block, and, after a waiting time T, the electron spins are saturated. We used a train of small flip-angle pulses and delays. A second spin lock fulfilling the NOVEL condition then leads to nuclear–electron transfer. Note that no $\pi/2$ pulse is needed at this point. The electron polarisation builds up along the spin-lock axis and can be read out again by a simple echo. While this detection subsequence is formally equivalent to a notched echo (Ponti and Schweiger, 1994), the build-up of electron magnetisation during the high-turning-angle pulse differs.

Figure 2b shows the echo intensity as a function of the nutation frequency of the *first* spin lock, while the power of the second spin lock was fixed at the optimum (i.e. the minimum determined in Fig. 1b). Clearly, the signal is highest if the spin-lock nutation frequency matches the proton Larmor frequency. Interestingly, a signal can be recovered even if T is set to 20 ms (red line), which corresponds to $T > 5 \cdot T_{1,e}$. Note that a plus/minus phase cycle was used on the very first $\pi/2$ pulse and the detection phase. This proves that there is a correlation between the first NOVEL block and the detected signal, even if $T \gg T_{1,e}$. These findings indicate that nuclear polarisation is generated during the first NOVEL block, even without direct proton NMR detection.

As mentioned earlier, the effective Hamiltonian during forward and reverse DNP is the same, and this leads to an oscillation of the difference in polarisation. Figure 3a compares the *depolarisation* curve (black) of Fig. 1c with the *repolarisation* curve (red). The latter was obtained by fixing the length of the first transfer to the minimum of the depolarisation curve (184 ns) and varying the length of the second

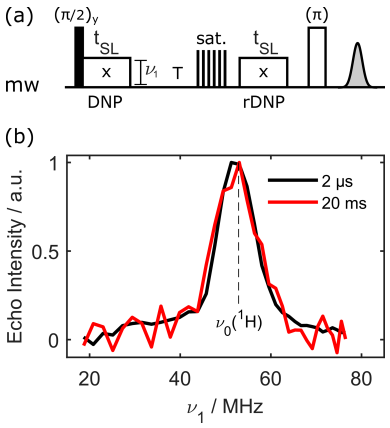

Figure 2. Transferring polarisation to nuclei and back to electrons. Panel **(a)** displays the pulse sequence. After an initial DNP step and a waiting time T, the electron spins are saturated. The next DNP step then leads to nuclear–electron polarisation transfer. The electron polarisation, which builds up along the spin-lock axis, can be read out with an echo. Timing details are given in Sect. 6. Panel **(b)** shows the repolarisation matching for 100 µM OX063 in protonated water/glycerol at 80 K. The microwave power during the first transfer is swept, while the second transfer is kept the same with optimised parameters. Different colours indicate different values of T.

transfer. The power of both transfers was set to the NOVEL condition. The repolarisation curve is essentially the inverse of the depolarisation curve, although only a maximum of 1 % signal intensity relative to a Hahn echo could be achieved in this fully protonated sample.

This efficiency is quite poor. We assume that multi-spin effects involving several nuclei play a role in this (Henstra and Wenckebach, 2008). Additionally, the nutation frequency of the spin lock is inhomogeneously broadened because the microwave power is different in different positions inside the resonator (as visible in Fig. 2b as well as in nutation spectra in the Supplement).

A simple way to improve the robustness of NOVEL with respect to microwave inhomogeneity is to use ramped-amplitude (RA) NOVEL (Can et al., 2017). In this case, the polarisation is transferred adiabatically, analogous to RA CP (Hediger et al., 1994), which improves robustness and potentially increases the maximal polarisation that can be transferred (details about RA NOVEL can be found in the Supplement). Figure 3b shows the repolarisation curves using RA NOVEL both in fully protonated (black) and fully deuterated (red) solvent. The first polarisation step was optimised for both solvents individually, also using RA NOVEL. In the case of fully deuterated solvent, relative echo intensities of 10 % could be achieved after the two transfer steps. This is already much more promising for future uses. Note that even in deuterated solvent, there are still 48 non-exchangeable protons in OX063. We speculate that the transfer efficiency

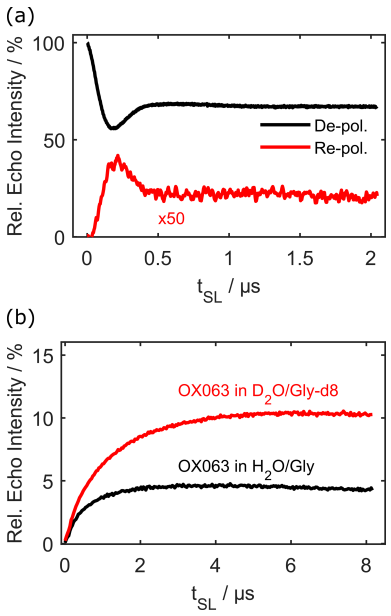

Figure 3. Repolarisation dynamics. Panel **(a)** displays a comparison of the depolarisation curve in Fig. 1c with the corresponding repolarisation curve that was measured by sweeping the length of the second DNP step while keeping the first transfer fixed with optimised parameters for 100 µM OX063 at 80 K in protonated solvent. Panel **(b)** shows repolarisation curves using ramped-amplitude (RA) NOVEL in different solvents. In both instances, the protons were polarised and depolarised. All data were measured with 100 µM OX063 at 80 K.

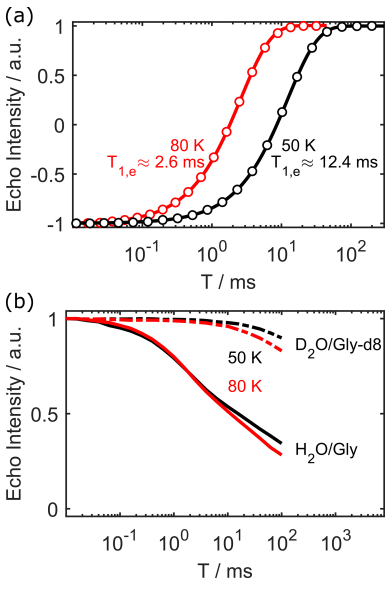

Figure 4. Electron inversion recovery **(a)**, and decay of nuclear polarisation **(b)** at 50 and 80 K for 100 µM OX063. $T_{1,e}$ is unaffected by deuteration of the solvent.

could be improved for less-abundant nuclei, but experiments are needed to test this hypothesis.

4 Proton polarisation decay

We now turn our attention to the decay of the nuclear polarisation during the waiting time T in Fig. 2a.

As a comparison and benchmark, we first measured the longitudinal electron spin relaxation time ($T_{1,e}$) at temperatures of 50 and 80 K. The inversion recovery curves and best fits (single exponential) are shown in Fig. 4a. As expected from results in the literature (Chen et al., 2016), $T_{1,e}$ is strongly dependent on temperature.

We then measured the decay of proton polarisation during the interval T for 100 µM OX063 in both protonated and fully deuterated solvent. The results are shown in Fig. 4b. We only measured up to 100 ms due to software and AWG memory constraints. These constraints did not pose limitations in any of our previous work, as repetition times in EPR are usually 1 to 2 orders of magnitude shorter. We expect to solve this problem in the near future. Even without full characterisation of the decay curve, some qualitative results can still be deduced. First, the proton polarisation decay is much slower than $T_{1,e}$, even in fully protonated solvent. Second, there is only a weak temperature dependence of the proton polarisation decay between 50 and 80 K. Lastly, there is a very pronounced difference between deuterated and protonated solvent. In the deuterated case, there is still 90 % of the polarisation left after 100 ms. Note that simple (stretched) exponential functions did not give satisfying fits to the experimental data. While sums of stretched exponentials might work, we would like to refrain from naïve fittings in the absence of complete experimental data (i.e. decayed to zero) and adequate quantitative models. Such a model might look similar to Stern et al. (2021) and could be the topic of future work. In the context of this work, the clear qualitative differences suffice to illustrate that our method can be used to characterise the polarisation dynamics of protons close to the paramagnetic centre. We tentatively assign the faster proton polarisation decay in protonated solvent to increased nuclear spin diffusion away from the unpaired electron in protonated solvent.

Typical DNP measurements are conducted with substantially higher electron spin concentrations than those used in the experiments thus far (100 µM). Therefore, we tested the influence of much higher concentrations, i.e. 5 mM (see Fig. 5a). Clearly, the proton polarisation decay is accelerated at higher electron spin concentrations. Additionally, the slight temperature dependence between 50 and 80 K vanishes at these elevated concentrations. Note that $T_{1,e}$ is unchanged between 100 µM and 5 mM (see the Supplement). However, we would like to point out that the broadband chirp pulses used for the inversion recovery measurements are able to invert the complete EPR spectrum, effectively eliminating the influence of electron spin spectral diffusion on the apparent

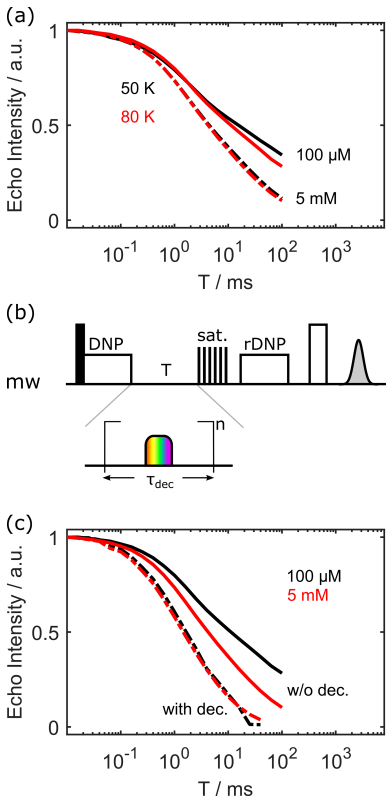

Figure 5. Panel **(a)** outlines the influence of the electron spin concentration on the proton polarisation decay. Panel **(b)** shows the sequence to investigate the effect of electron decoupling during the waiting time T. A chirp pulse inverts the electron spins every τ_{dec}. This is repeated $n = T/\tau_{dec}$ times. Panel **(c)** visualises the effect of electron decoupling. Solid lines denote that no decoupling was used during time T, and dashed lines denote that the electron spins were inverted every $\tau_{dec} = 30\,\mu s$ with an adiabatic chirp pulse for 100 µM OX063 at 80 K.

value of $T_{1,e}$. This is not always the case when measuring $T_{1,e}$.

Last but not least, we wanted to test if a periodic inversion of the electron spin during the waiting time T might accelerate the polarisation decay of nearby protons. The sequence is shown in Fig. 5b. Loosely speaking, we hypothesised that this periodic inversion would act as a hyperfine decoupling (Jeschke and Schweiger, 1997). Differences in hyperfine couplings (partially) truncate nuclear–nuclear flip-flops, leading to the notion of the "spin diffusion barrier" (Khutsishvili, 1963). Thus, eliminating or reducing the hyperfine couplings should increase the spin diffusion rate away from the paramagnetic centre. Indeed, this is what we observed. Figure 5c shows the proton polarisation decay without any hyperfine decoupling (solid lines) and with periodic inversion of the electron spins every 30 µs with an adiabatic chirp pulse, both for 100 µM and 5 mM OX063 concentration. In both cases, the periodic inversion increases the decay rate of the proton polarisation. Interestingly, with periodic inversion every 30 µs, there is no longer a difference between low and high concentrations. Together, these results suggest that electron–electron interactions influence nuclear spin diffusion away from the paramagnetic centre, as already discussed in Wolfe (1973). Note that a decoupling period of $\tau_{dec} = 30\,\mu s$ is not at all sufficient to completely suppress the hyperfine couplings, which can be in the megahertz (MHz) range. It would be better to invert much more often. However, we did not want to risk harming our microwave amplifier, as its specifications are given for much longer recovery periods. On the other hand, we would like to point out that the matrix element in the Hamiltonian that quenches the nuclear spin diffusion is given by the *difference* in hyperfine coupling values of the two nuclear spins, not by the absolute values.

5 Conclusion and outlook

In conclusion, we demonstrated that it is possible to transfer polarisation not only from electron spins to nuclear spins (DNP) but also back (reverse DNP). Using trityl OX063 in deuterated water/glycerol, an overall efficiency for both transfers of 10 % can be achieved with RA NOVEL. The nuclear polarisation is much longer-lived than the longitudinal relaxation time of the electrons ($T_{1,e}$). The former lifetime is strongly dependent on the deuteration of the solvent and weakly dependent on the electron spin concentration (between 100 µM and 5 mM). Periodic inversion of the electron spins every 30 µs leads to an increased proton polarisation decay, which we tentatively assign to an increased spin diffusion rate away from the paramagnetic centre under hyperfine decoupling.

This work is a proof of principle for the feasibility of DNP and reverse DNP for the indirect detection of nuclei. We can envisage several ways forward, and these are outlined in the following.

The investigation of the influence of different parameters, such as temperature, deuteration degree, and electron spin concentration, is only qualitative in this work. A systematic screen over a larger parameter range might give very valuable insight into nuclear spin dynamics for nuclei close to the paramagnetic centre. These nuclei are notoriously difficult to access experimentally. One could also combine our approach with standard DNP measurements under the same conditions, with the same parameters for polarisation transfer. Selective inversion experiments using radio frequency pulses on nuclei between the DNP and reverse DNP might give information about which nuclei actually contribute to the DNP enhancement of the bulk.

Another direction we foresee is to use our indirect detection approach for ENDOR-type experiments. In the conventional Mims and Davies ENDOR experiments, one generates longitudinal electron–nuclear two-spin order, not "pure" nuclear polarisation. Another established but less common EN-

DOR variant, namely cross-polarisation (CP) ENDOR (Rizzato et al., 2013), does generate nuclear polarisation, but the read-out is again achieved via longitudinal two-spin order and selective detection of one electron spin transition. It is not obvious how the sensitivity of ENDOR experiments with DNP and reverse DNP will compare to established sequences; therefore, this needs to be tested experimentally. We expect at least some advantages, especially in combination with hyperfine decoupling and time-domain ENDOR.

When going to higher fields and frequencies, the NOVEL condition will be difficult or impossible to achieve, as the necessary microwave (mw) power is not available. In this case, it might be possible to use other pulsed DNP variants, such as electron–nuclear CP (Weis and Griffin, 2006), off-resonance NOVEL (Jain et al., 2017), or the adiabatic solid effect (Tan et al., 2020). All of these have a lower scaling factor (i.e. a slower transfer) than NOVEL; however, as the maximum transfer in this work with constant-amplitude NOVEL is already achieved after < 200 ns, a lower scaling factor might still achieve an appropriate amount of polarisation transfer. We expect that further development of modulated sequences such as TOP (time-optimised pulsed) DNP (Tan et al., 2019c), XiX (X-inverse-X) DNP (Redrouthu and Mathies, 2022), or BEAM (broadband excitation by amplitude modulation) DNP (Wili et al., 2022) will also facilitate the use of reverse DNP at higher frequencies, at least in the W-band (≈ 95 GHz). BEAM-DNP has been demonstrated for the high-power regime, but it would also work at lower power if the modulation frequency was increased – again at the expense of a lower scaling factor.

In this work, we only used a narrow-line trityl radical. For radicals with a broader EPR spectrum, such as nitroxides, the bandwidth of the mw sequence will be smaller than the total spectral width. In this case, the experiment should still work *in principle*. Only a fraction of the electron spins will be excited, leading to orientation selection (Rist and Hyde, 1970), commonly encountered in pulse EPR experiments. In this case, an increased bandwidth of the mw sequence should lead to increased sensitivity.

6 Materials and methods

All measurements were conducted on a home-built Q-band (35 GHz, 1.2 T) EPR spectrometer based on a fast AWG and custom-written control software (Doll and Jeschke, 2017). Pulses were amplified using a 150 W travelling-wave tube (TWT) amplifier from Applied Systems Engineering. Temperature was controlled with a helium flow cryostat. We used a home-built broadband resonator with high conversion factor, allowing for electron spin nutation frequencies of about 100 MHz (Tschaggelar et al., 2017). The OX063 samples were obtained from GE Healthcare. We always used a 1 : 1 by volume mixture of water and glycerol as solvent, which was either fully protonated or fully deuterated (as indicated in each figure). For each sample, 7 µL was transferred into a 1.6 mm (outer diameter) quartz EPR tube, which was shock-frozen in liquid nitrogen and inserted into the cold resonator.

The $\pi/2$ and π pulses were generally set to 4 and 8 ns respectively. The delay in the echo detection was set to 300 ns. A plus/minus phase cycle for the very first pulse and the detection was used. Saturation was achieved by a train of 15 pulses of 10 ns duration, spaced by delays of 2 µs. The flip angle of the pulses was about 70 °. If not stated otherwise, the time T between the initial DNP step and the saturation was set to 2 µs. The reverse DNP was started 2 µs after the saturation train.

The optional chirp pulses for hyperfine decoupling during time T were of 200 ns length, covered a bandwidth of ± 150 MHz (linear frequency sweep), and were applied at full power (not quite 100 MHz ν_1). The edges of the amplitude modulation were smoothed with a quarter sine wave with a length of 20 ns.

Inversion recovery experiments were measured with the following sequence: chirp $- T - \pi/2 - \tau - \pi - \tau -$ echo. The same chirp pulse as described above was used.

The shot repetition time was usually set to 10 ms for the measurements shown here conducted at 80 K. If the total sequence length was longer than this, the shot repetition time was set to twice the total sequence length plus an additional 20 ms. The number of shots and averages for each figure are given in the Supplement. Individual averages were saved to check for any systematic saturation behaviour. For the measurements with deuterated solvent, phase cycling and presaturation of the nuclei close to unpaired electrons by multiple electron saturation and reverse DNP was used to mitigate the effects of very slow nuclear relaxation/spin diffusion (see the Supplement).

Code and data availability. All data and code used in this paper are archived on Zenodo: https://doi.org/10.5281/zenodo.6684677 (Wili, 2022).

Supplement. The supplement related to this article is available online at: https://doi.org/10.5194/mr-3-161-2022-supplement.

Author contributions. NW designed the research, measured and analysed all data, and wrote the initial draft of the manuscript. GJ and JHAL discussed the results and edited the manuscript.

Competing interests. Jan Henrik Ardenkjær-Larsen is the owner of Polarize ApS; Polarize ApS manufactures a dDNP polarizer, but the Polarize ApS instrument was not used in this work. Nino Wili and Gunnar Jeschke declare that they have no conflict of interest.

Acknowledgements. Matthias Ernst is acknowledged for helpful discussions about spin diffusion measurements in NMR.

Financial support. This research has been supported by the Eidgenössische Technische Hochschule Zürich (grant no. ETH-48 16-1).

Review statement. This paper was edited by Geoffrey Bodenhausen and reviewed by Marina Bennati, Daniella Goldfarb, and Frédéric Mentink-Vigier.

References

Bornet, A., Milani, J., Vuichoud, B., Perez Linde, A. J., Bodenhausen, G., and Jannin, S.: Microwave frequency modulation to enhance Dissolution Dynamic Nuclear Polarization, Chem. Phys. Lett., 602, 63–67, https://doi.org/10.1016/j.cplett.2014.04.013, 2014.

Can, T. V., Walish, J. J., Swager, T. M., and Griffin, R. G.: Time domain DNP with the NOVEL sequence, J. Chem. Phys., 143, 054201, https://doi.org/10.1063/1.4927087, 2015.

Can, T. V., Weber, R. T., Walish, J. J., Swager, T. M., and Griffin, R. G.: Ramped-amplitude NOVEL, J. Chem. Phys., 146, 154204, https://doi.org/10.1063/1.4980155, 2017.

Chen, H., Maryasov, A. G., Rogozhnikova, O. Y., Trukhin, D. V., Tormyshev, V. M., and Bowman, M. K.: Electron spin dynamics and spin–lattice relaxation of trityl radicals in frozen solutions, Phys. Chem. Chem. Phys., 18, 24954–24965, https://doi.org/10.1039/C6CP02649D, 2016.

Doll, A. and Jeschke, G.: Wideband frequency-swept excitation in pulsed EPR spectroscopy, J. Magn. Reson., 280, 46–62, https://doi.org/10.1016/j.jmr.2017.01.004, 2017.

Ernst, R. R., Bodenhausen, G., and Wokaun, A.: Principles of nuclear magnetic resonance in one and two dimensions, Clarendon Press, Oxford, ISBN 0-19-855629-2, 1987.

Gao, C., Alaniva, N., Saliba, E. P., Sesti, E. L., Judge, P. T., Scott, F. J., Halbritter, T., Sigurdsson, S. T., and Barnes, A. B.: Frequency-chirped dynamic nuclear polarization with magic angle spinning using a frequency-agile gyrotron, J. Magn. Reson., 308, 106586, https://doi.org/10.1016/j.jmr.2019.106586, 2019.

Harmer, J. R.: Hyperfine Spectroscopy – ENDOR, eMagRes, 5, 1493–1514, https://doi.org/10.1002/9780470034590.emrstm1515, 2016.

Hediger, S., Meier, B., Kurur, N. D., Bodenhausen, G., and Ernst, R.: NMR cross polarization by adiabatic passage through the Hartmann–Hahn condition (APHH), Chem. Phys. Lett., 223, 283–288, https://doi.org/10.1016/0009-2614(94)00470-6, 1994.

Henstra, A. and Wenckebach, W. T.: The theory of nuclear orientation via electron spin locking (NOVEL), Mol. Phys., 106, 859–871, https://doi.org/10.1080/00268970801998262, 2008.

Henstra, A., Dirksen, P., Schmidt, J., and Wenckebach, W. T.: Nuclear spin orientation via electron spin locking (NOVEL), J. Magn. Reson., 77, 389–393, https://doi.org/10.1016/0022-2364(88)90190-4, 1988.

Hovav, Y., Feintuch, A., Vega, S., and Goldfarb, D.: Dynamic nuclear polarization using frequency modulation at 3.34 T, Jm Magnm Resonm, 238, 94–105, https://doi.org/10.1016/j.jmr.2013.10.025, 2014.

Jain, S. K., Mathies, G., and Griffin, R. G.: Off-resonance NOVEL, J. Chem. Phys., 147, 164201, https://doi.org/10.1063/1.5000528, 2017.

Jain, S. K., Yu, C. J., Wilson, C. B., Tabassum, T., Freedman, D. E., and Han, S.: Dynamic Nuclear Polarization with Vanadium(IV) Metal Centers, Chem., 7, 421–435, https://doi.org/10.1016/j.chempr.2020.10.021, 2021.

Jeschke, G. and Schweiger, A.: Hyperfine decoupling in electron spin resonance, J. Chem. Phys., 106, 9979–9991, https://doi.org/10.1063/1.474073, 1997.

Kaminker, I. and Han, S.: Amplification of Dynamic Nuclear Polarization at 200 GHz by Arbitrary Pulse Shaping of the Electron Spin Saturation Profile, J. Phys. Chem. Lett., 9, 3110–3115, https://doi.org/10.1021/acs.jpclett.8b01413, 2018.

Khutsishvili, G.: Spin Diffusion, Magnetic Relaxation, and Dynamic Polarization of Nuclei, Soviet Phys.-JETP, 16, 1540–1543, 1963.

Lilly Thankamony, A. S., Wittmann, J. J., Kaushik, M., and Corzilius, B.: Dynamic nuclear polarization for sensitivity enhancement in modern solid-state NMR, Prog. Nucl. Magn. Reson. Spectrosc., 102–103, 120–195, https://doi.org/10.1016/j.pnmrs.2017.06.002, 2017.

Mathies, G., Jain, S., Reese, M., and Griffin, R. G.: Pulsed Dynamic Nuclear Polarization with Trityl Radicals, J. Phys. Chem. Lett., 7, 111–116, https://doi.org/10.1021/acs.jpclett.5b02720, 2016.

Ni, Q. Z., Daviso, E., Can, T. V., Markhasin, E., Jawla, S. K., Swager, T. M., Temkin, R. J., Herzfeld, J., and Griffin, R. G.: High Frequency Dynamic Nuclear Polarization, Accounts Chem. Res., 46, 1933–1941, https://doi.org/10.1021/ar300348n, 2013.

Ponti, A. and Schweiger, A.: Echo phenomena in electron paramagnetic resonance spectroscopy, Appl. Magn. Reson., 7, 363–403, https://doi.org/10.1007/bf03162620, 1994.

Redrouthu, V. S. and Mathies, G.: Efficient Pulsed Dynamic Nuclear Polarization with the X-Inverse-X Sequence, J. Am. Chem. Soc., 144, 1513–1516, https://doi.org/10.1021/jacs.1c09900, 2022.

Rist, G. H. and Hyde, J. S.: Ligand ENDOR of Metal Complexes in Powders, J. Chem. Phys., 52, 4633–4643, https://doi.org/10.1063/1.1673696, 1970.

Rizzato, R., Kaminker, I., Vega, S., and Bennati, M.: Cross-polarisation edited ENDOR, Mol. Phys., 111, 2809–2823, https://doi.org/10.1080/00268976.2013.816795, 2013.

Shimon, D. and Kaminker, I.: Electron Spin Effects in Static DNP with Broadband Excitation, eMagRes, 9, 309–332, 2020.

Stern, Q., Cousin, S. F., Mentink-Vigier, F., Pinon, A. C., Elliott, S. J., Cala, O., and Jannin, S.: Direct observation of hyperpolarization breaking through the spin diffusion barrier, Sci. Adv., 7, 1–14, https://doi.org/10.1126/sciadv.abf5735, 2021.

Tan, K. O., Jawla, S., Temkin, R. J., and Griffin, R. G.: Pulsed dynamic nuclear polarization, eMagRes, 8, 339–352, 2019a.

Tan, K. O., Mardini, M., Yang, C., Ardenkjær-Larsen, J. H., and Griffin, R. G.: Three-spin solid effect and the spin diffusion barrier in amorphous solids, Sci. Adv., 5, eaax2743, https://doi.org/10.1126/sciadv.aax2743, 2019b.

Tan, K. O., Yang, C., Weber, R. T., Mathies, G., and Griffin, R. G.: Time-optimized pulsed dynamic nuclear polarization, Sci. Adv., 5, eaav6909, https://doi.org/10.1126/sciadv.aav6909, 2019c.

Tan, K. O., Weber, R. T., Can, T. V., and Griffin, R. G.: Adiabatic Solid Effect, J. Phys. Chem. Lett., 11, 3416–3421, https://doi.org/10.1021/acs.jpclett.0c00654, 2020.

Tschaggelar, R., Breitgoff, F. D., Oberhänsli, O., Qi, M., Godt, A., and Jeschke, G.: High-Bandwidth Q-Band EPR Resonators, Appl. Magn. Reson., 48, 1273–1300, https://doi.org/10.1007/s00723-017-0956-z, 2017.

van den Heuvel, D. J., Henstra, A., Lin, T. S., Schmidt, J., and Wenckebach, W. T.: Transient oscillations in pulsed dynamic nuclear polarization, Chem. Phys. Lett., 188, 194–200, https://doi.org/10.1016/0009-2614(92)90008-B, 1992.

Weis, V. and Griffin, R.: Electron-nuclear cross polarization, Solid State Nucl. Mag., 29, 66–78, https://doi.org/10.1016/j.ssnmr.2005.08.005, 2006.

Wili, N.: Raw Data and Evaluation Scripts for: "Reverse Dynamic Nuclear Polarisation for indirect detection of nuclear spins close to unpaired electrons", Zenodo [data set], https://doi.org/10.5281/zenodo.6684677, 2022.

Wili, N., Nielsen, A. B., Völker, L. A., Schreder, L., Nielsen, N. C., Jeschke, G., and Tan, K. O.: Designing broadband pulsed dynamic nuclear polarization sequences in static solids, Sci. Adv., 8, eabq0536, https://doi.org/10.1126/sciadv.abq0536, 2022.

Wolfe, J. P.: Direct Observation of a Nuclear Spin Diffusion Barrier, Phys. Rev. Lett., 31, 907–910, https://doi.org/10.1103/physrevlett.31.907, 1973.